15th CIRP Conference on Modelling of Machining Operations

Prediction of the 3D Surface Topography after Ball End Milling and its Influence on Aerodynamics

B. Denkena[a], V. Böß[a], D. Nespor[a*], P. Gilge[b], S. Hohenstein[b], J. Seume[b]

aInstitute of Production Engineering and Machine Tools (IFW), Leibniz Universität Hannover, Germany
bInstitute of Turbomachinery and Fluid Dynamics (TFD), Leibniz Universität Hannover, Germany

* Corresponding author. Tel.: +49 511 4299; fax: +49 511 5115. *E-mail address:* nespor@ifw.uni-hannover.de

Abstract

The surface topography of milled workpieces often defines their performance. One example is blades in turbine engines, where the topography defines the flow losses. This type of complex goods is often machined by ball end mills, either for manufacture or repair. The literature offers various model types to predict the surface topography in order to design a machining process without prior experiment. The most accurate models use the real kinematics of the process and blend the tool with the workpiece. But this type of surface prediction ignores the differences between the reality and the simulation due to vibrations, tool chipping etc. This paper presents a combined approach using the kinematic topography from the machining simulation and adds a stochastic topography based on empirical data. It could be shown, that the usage of the stochastic topography greatly affects the flow losses and thus cannot be ignored.

Keywords: Milling; Topography; Simulation

1. Introduction

Milling is one of the most commonly used processes for repair and manufacturing of high functional parts in the aerospace industry [1, 2]. Especially ball nose end mills are generally applied for complex blade and vane airfoil geometries due to the flexibility of this process, e.g. the selectable cutter orientations to the surface. This flexibility enables a free definition of the milled surface topography by suitable choice of the milling cutters and 5-axis process strategy. It is known that a suitable choice of process parameters for 5-axis ball end milling can lead to surface qualities which are comparable to grinding, as shown by Markworth [4] and Knobel [5]. The disadvantage of ball end milling is the poor productivity compared to end milling. Due to the impact of the surface topography on the functional performance of parts [6], extensive research work has been carried out to predict the surface topography before the experiment for various cutting processes. The predictive models can be characterized as empirical, analytical/numerical and material removal simulations. One example of an empirical model was presented by Vakondios et al., where mathematical regression between the process parameters and the resulting surface parameter Rz is used. Empirical models are very accurate and easy to use, but are limited to the experimental scope. Analytical models mathematically describe the shape [4, 5] and/or the trajectory of the cutting edges [7]. For instance, the analytical model of Arizmendi et al. show the importance of tool runout and its impact on surface topography [7]. However, the analytical equations can get too complex to handle by adding more simulation features, such as vibrations or special tool shapes etc. Therefore, the third group represents the material removal simulations (MRS), where the workpiece is represented with voxel, dexel or solid modelling such as constructive solid geometry. The simulation with MRS is generally slower compared to analytical and empirical models, but allows the highest flexibility. It has been shown by Liu et al. that the movement of the cutting edge is a superior approach in terms of accuracy compared to a Boolean subtraction between workpiece and the rotation body of the milling tool, e.g. a sphere for ball end mills [8]. The resulting surfaces after MRS are perfectly

smooth without stochastic influences. This often leads to underestimated surface parameters [8-10]. But several investigations concerning the interaction of the wall and the near-wall flow have shown that the topography of the wall surface significantly influences the aerodynamic losses that occur on blades or vanes [11-14]. Particularly the height and the shape of the surface structure, as well as their alignment with respect to the direction of the flow can increase the overall friction loss [15, 16]. Even relatively small structures may have an effect on the friction between the wall and the fluid, as is exemplified by riblets [17]. Due to their shape and direction on the surface they reduce the aerodynamic losses. This suggests that every change of the surface topology can have an influence on the aerodynamic loss behaviour of an airfoil.

In order to enhance MRS for aerodynamic purpose this paper presents a combined approach with an empirical model which considers stochastic influences such as tool vibrations, chipped cutting edge, adhesion etc. It is based on the approach of the model presented by Denkena et al. [18]. An overview of the approach is given in figure 1. Section 2.1 presents the experiments and the used equipment. All measured surfaces of section 2.1 are simulated in section 2.2 using the MRS CutS [19]. The results of these simulations are called "kinematic topography". In section 2.3 the differences between the measurements and experiments are described and modelled empirically using statistical methods. The combination of the kinematic simulation and the empirical model leads to an enhanced combined simulation. In section 3, the flow loss for aerodynamic applications is described and compared in order to evaluate the need for considering stochastic influences.
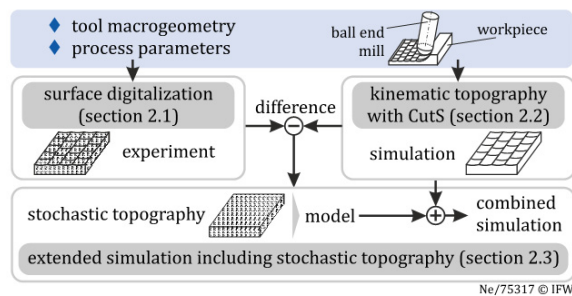

Fig. 1. Methods and approach

2. Surface topography after ball end milling

2.1. Experimental setup and surface digitalization

Flat workpieces of titanium alloy Ti-6A-4V were selected for this study. All milling experiments were performed on the 5-axis milling centre DMU125P. A ball end mill cutter of the type CoroMill R216-10A16-050 with one indexable insert was used, which was exchanged after a set of five experiments to exclude tool wear. Process forces were measured with a three-component force dynamometer, type 9257B. In addition to the experiments described in [18], the lead angle λ and tilt angle τ were varied and higher feed per tooth f_z was used all due to their impact on the surface topography. All experiments were performed by a one-factor-at-time process plan by assuming negligible interdependency between the parameters. Each experiment was performed twice to moderate statistical influences, which results in a total number of 50 experiments. The white light confocal microscope type µsurf was used to measure the resulting surface topography after machining. It is important for the presented approach that the digitalized surface topographies are without measurement artefacts or defects, which would have a crucial impact on the approach (compare figure 1). Goeke et al. compared different object lenses for measurements with the same white light confocal microscope and their impact on the results [20]. They highlighted that only tactile measurements are standardised for surface parameters such as Rz or Ra. No general recommendation can be drawn for the right choice of object lenses or filter options due to their dependency on the measured surface. Therefore, standardised tactical measurements using multiple parallel measurements for a 3D representation are compared with the white light confocal microscope using different object lenses and filter options. The measured workpiece is a calibration standard with the same roughness values and reflection as the milled surfaces. It has been shown that a lens of 50x magnification and a high-pass gauss filter with a wavelength of $\lambda_{\mathrm{filt}} = 800$ µm is suitable for measuring the milled surfaces, as shown in figure 2. The resolution of the 50x magnification for a 1.4 x 1.4 mm surface is 2226 x 2226 pixel with a maximum measurement uncertainty of $\mu_{90\%} = 0{,}32$ µm for the parameter Rz by using a confidence interval of 90 %. The maximum relative measurement uncertainty for the parameter Rz is $f_{90\%} = 6{.}8$ %.
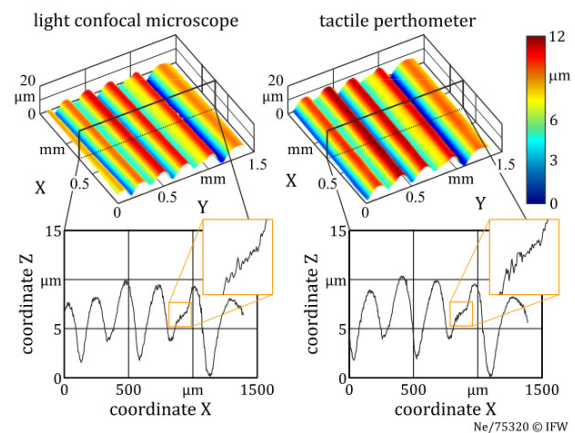

Fig. 2. Comparison between optical and tactile measurements

2.2. Kinematic simulation with CutS and differentiation

Table 1. Process matrix for the experiments

	cutting speed v_c [m/min]	feed/ tooth f_z [mm]	step-over b_r [mm]	depth of cut a_p [mm]	lead angle λ [°]	tilt angle τ [°]
range of variations	10 to 160	0.09 to 0.45	0.2 to 0.6	0.2 to 1.2	-15 to +45	-15 to +45
number of variations	3	5	5	3	5	5

In order to simulate the kinematic surface topography the MRS CutS, developed by IFW, is used. This type of MRS discretizes the workpiece into two-dimensional lines, called dexel or Z-map grid, which is shown in figure 3 and described in [18, 19]. The tool is intersected with the workpiece by a Boolean operation applied to each dexel which is shortened, divided or removed. In order to consider the real tool kinematics, the tool rotates with the spindle speed *n* and the feed velocity v_f in the simulation. An integrated emulation of an NC-Control moves the axes of the underlying machine kinematic using the same type of G-Code as for the milling centre. At the end of the simulation the end points of all dexels represent the shape the kinematic topography.

All cutting parameters, which are significant for the surface generation, such as the lead angle λ, the tilt angle τ, the feed per tooth f_z and the step over b_r (offset between two cutting paths) are considered in the simulation as depicted in figure 3. For instance the depth of cut a_p has no influence on the final surface, except for the Z-level.

It is essential for good simulation results to use a detailed CAD model of the cutter, which has to consider runout as shown by Arizmendi et al. [7]. Therefore the cutting edge and plane surfaces of the insert were measured by a coordinate measuring machine, type Leitz PMM 866. The measured X-Y-Z coordinates were imported to a CAD-software to establish a detailed solid model of the insert, as shown in the upper part of figure 4. Furthermore, the position of the real tool axis was determined by the coordinate measuring machine too. The CAD model and the tool axis position were imported to the CutS environment. The size of the workpiece for the topography simulation complies with the actual measurement of the confocal microscope. In order to accomplish the Boolean operation of the virtual material removal, the geometrical workpiece model was transferred to a discrete z-map model (resolution 512 x 512). Due to time discretization during simulation the angular step of the trochoidal cutting edge movement determines the accuracy of the computed surface. Therefore, the angular step has been analytically calculated and optimized, which leads to a maximum deviation in z-direction of 1.71 µm compared to continuous tool movement. The datasets from the whitelight confocal microscope and the kinematic topography simulation are available as point clouds. To align both datasets to each other, an iterative closest point algorithm (ICP) was applied based on the work of Rusinkiewicz and Levoy [21]. In contrast to the results in [18], the alignment was not successful due to the increased feed per tooth f_z. In the lower part of figure 4 the measurement and the corresponding simulation are shown for a set of process parameters with same feed per tooth f_z and step over b_r values. Due to the kinematics and the geometry of the cutting edge the surface shows scallops with local maxima (red) and minima (blue). All local minima are marked with white crosses for a better overview.
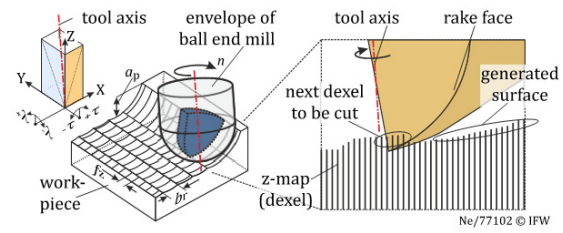

Fig. 3. Process parameters z-map model of the workpiece

It can be seen, that the offset between the local minima is changing in feed direction for the measurements, whereas the simulation has constant offsets. This is due to slightly changing spindle speeds during the experiment, which changes the offset randomly. The offset in the simulation is determined by the spindle rotation speed and time of tool retraction. Figuratively speaking the orientation of the white crosses to each other in step over direction is defined by the angle of rotation of the spindle when entering the workpiece. To cope with that problem only one row is used for the ICP alignment between measurements and simulation, indicated with the dotted rectangle in figure 4. In order to obtain the difference between the kinematic topography of the simulation and the measured topography, the surfaces of one row are aligned to each other and subtracted afterwards. This result is called measured "stochastic topography" in the following. The parameter set with a lead angle λ = 0° and tilt angle τ = 0° is not used for subtraction due to the high differences between measurement and simulation because of the engaged tool tip with a cutting speed of v_c = 0 m/min. This leads to ploughing and rubbing instead of cutting, which results in tip marks generated on the surface and may cause tool damage as described by Ozturk et al. [22].
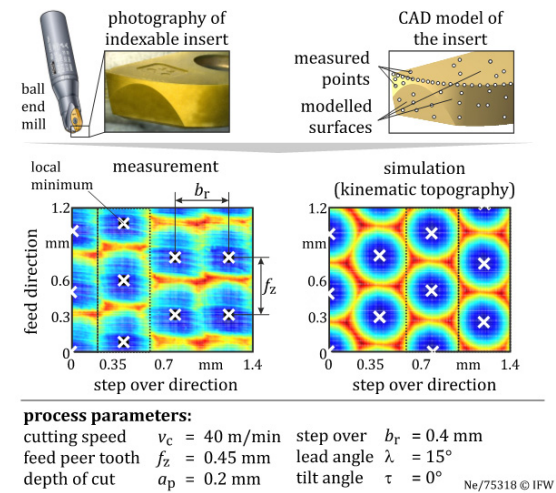

process parameters:
cutting speed v_c = 40 m/min   step over b_r = 0.4 mm
feed peer tooth f_z = 0.45 mm   lead angle λ = 15°
depth of cut a_p = 0.2 mm   tilt angle   τ = 0°

Fig. 4. Simulation and measurement of surface topography

2.3. Extended simulation including stochastic topography

This section describes a method to characterize the difference between the actual surface topography and the geometrical simulation. The aim is firstly to describe the measured stochastic topographies by appropriate values and secondly to predict the stochastic topography with a suitable method. All measured stochastic topographies of the experiments are determined as described in section 2.2. For the prediction it is assumed that the stochastic topography has the same behavior in the feed and the step over direction. Actually this is a simplification of reality. The measured stochastic topographies determined in section 2.2 show slight grooves in feed direction which is most likely due to edge chipping, as shown by [23]. Nevertheless the differences caused by these simplifications are about $\Delta Rz \approx 1$ μm and thus are negligible.

It has to be mentioned that the irregularities of the stochastic topography cannot be described by a single number, but with a distribution function, which type is unknown. Whereas a Gaussian distribution is defined by two parameters, the standard deviation σ and the expectation μ, a general distribution is characterized by four distribution moments $\mu_1 - \mu_4$ as described by Hahn and Shapiro [24]. Analogous to Gaussian distribution the first distribution moment

$$\mu_1 = \frac{1}{n} \cdot \sum_{i=1}^{x} x_i \qquad (1)$$

is the expectation and the second distribution moment

$$\mu_2 = \frac{1}{n-1} \cdot \sum_{i=1}^{x} (x_i - \mu_1)^2 \qquad (2)$$

is the standard deviation, which describes the variance. The third distribution moment

$$\mu_3 = \frac{1}{n-1} \cdot \sum_{i=1}^{x} (x_i - \mu_1)^3 \qquad (3)$$

is the skewness which measures the asymmetry of the distribution. The fourth distribution moment

$$\mu_4 = \frac{1}{n-1} \cdot \sum_{i=1}^{x} (x_i - \mu_1)^4 \qquad (4)$$

is called kurtosis and it is a measure for the peakedness of a probability distribution. For this paper the distribution moments μ_2-μ_4 are used to describe the measured stochastic topography, because $\mu_1 = 0$ by definition. One example of such a distribution by real measurement data is shown in the upper part of figure 5, where all Z-values of the measured stochastic topography are depicted in a histogram.

All values of $\mu_2 - \mu_4$ for all measured stochastic topographies based on the cutting experiments are plotted against the cutting parameters listed in table 1. Quadratic regression functions are used to fit the values, which allow predicting $\mu_2 - \mu_4$ based on the cutting parameters, as indicated in the middle of figure 5. It shows that the roughness of the stochastic topography increases with an increased feed per tooth f_z and depth of cut a_p, which is most likely due to higher process forces and increased vibrations. The cutting speed v_c has no significant influence on the stochastic topography within the tested range. Small inclination angles show a lower stochastic influence neglecting the value of $\lambda = 0°$ and tilt angle $\tau = 0$ due to ploughing.
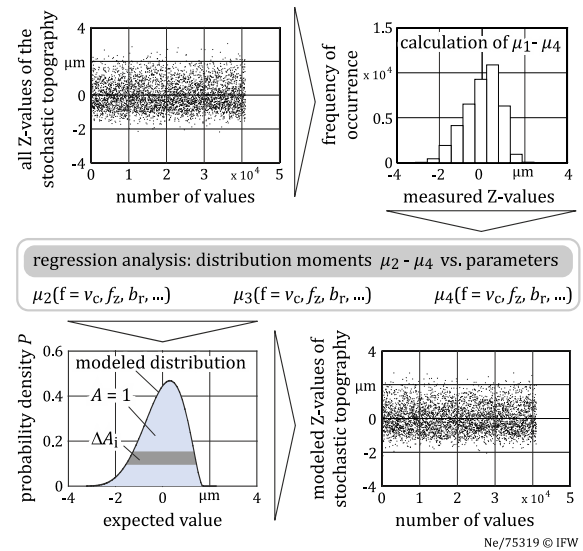

Fig. 5. Methodology for simulating stochastic topography

This effect can be explained by higher tool vibrations due to changed force vectors. The orientation of the force vectors are rather perpendicular to the tool axis using high inclination angles compared to lower inclination angles. Subsequently the distribution based on the distribution moments μ_2 - μ_4 is modelled using the Pearson distribution family [25]. One example of modeled distribution curve is shown in the lower left diagram of figure 5, which is the simulation of the upper histogram. A detailed description and its derivation can be found in literature [25, 26]. Afterwards the modelled distribution is converted to the values of stochastic topography by using random numbers. This method is described in [18] and it is based on the horizontal discretization of the distribution and the creation of pseudo-random numbers for each discrete area. The quantity of random numbers for each horizontal discretization is weighted with the quotient $\Delta A_i/A$, see figure 5. All random numbers are placed into an X-Y array, which leads to the simulated stochastic topography. One example of the simulated stochastic topography is shown in figure 6(B).

Adding the kinematic topography (A) with the stochastic topography (B) results in the combined simulation (C). In comparison to the measurement (D) it can be seen that the consideration of the stochastics does influence the appearance

of the topography and therefore will affect the flow losses during application.

All required surface parameters can be calculated using the superimposed profile. This is done exemplarily for the parameter Ra and Rz in figure 7 in comparison to a kinematic simulation without stochastic influence in feed direction. It can be seen, that the addition of the stochastic topography well improves the simulation of the kinematic topography. The proposed surface model simulates a topography profile including statistical influences, which are not negligible especially in finishing operations. Each plane and spatial parameter can be determined with the simulated topography profile by using the respective standard.
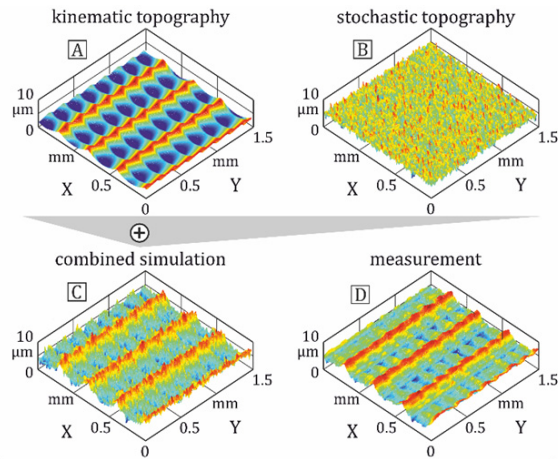
process parameters:

cutting speed	v_c	= 40 m/min	step over	b_r = 0.40 mm
feed peer tooth	f_z	= 0.18 mm	lead angle	λ = 15°
depth of cut	a_p	= 0.20 mm	tilt angle	τ = 45°

Ne/75321a © IFW

Fig. 6. Result of the combined approach to simulate realistic surface topographies after ball end milling

In this research Ti-6Al-4V has been used as the workpiece material. Whereas the kinematic simulation is independent from the workpiece material, the stochastic topography and the empiric equations will change for different materials, e.g. nickel based alloys.
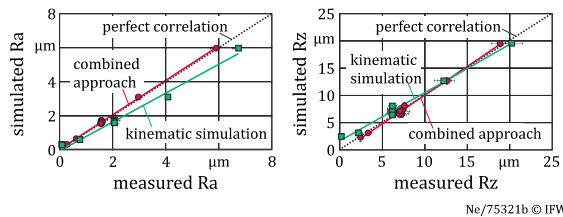

Fig. 7. Comparison of kinematic simulation and combined approach

3. Aerodynamics of milled surfaces

Numerical studies of two surfaces were performed to show the necessity for the presented approach combining the kinematic topography with a stochastic topography, with regard to fluid mechanical applications. The objective of the numerical studies was to estimate the influence of the added stochastic topography on the aerodynamic interaction between the fluid and the surface. The numerical computations include an ideal, kinematic and simulated surface and a combined, kinematic and stochastic surface. The simulations were performed with the same milling process parameters as in figure 6 and the dimensions of both surfaces are equal.

3.1. Numerical methods

Direct Numerical Simulations (DNS) were conducted using the fluid solver ChannelFOAM, which is part of the OpenFOAM Software Package. An advantage of this solver is the ability to compensate for the pressure drop due to friction. The compensation is realised by an imprinted pressure gradient and the result is a constant fluid velocity in the domain [27].

The computational domain consists of a cuboid-shaped channel with dimensions of $l_x = 6\delta \approx 1.4$ mm, $l_y = 2\delta$ and $l_z = 3\delta$ (δ = channel half height). In order to fit the dimensions of the surfaces under investigation, the domain was adjusted in the X- and Z- directions. The main flow is directed in the positive X-direction. The inlet and the outlet of the channel are cyclic, as are the side walls in Z-direction, resulting in a flow channel with infinite dimensions in the X- and Z-direction. The top and bottom boundaries of the channel are an ideal smooth wall and a rough surface, respectively. The simulated surfaces were placed on the rough (bottom) side of the channel. The smooth (top) side is used as a reference to determine the difference in the flow-wall-interactions of the smooth and rough surfaces. Polyhedral cells with an undefined shape are used for the discretization. The number of cells for each direction is: $N_{Cells,X} = 320$, $N_{Cells,Y} = 220$ and $N_{Cells,Z} = 160$. In order to discretize the near wall area the adjacent cells are smaller than those near the center of the channel. Therefore, the growth ratio of the cells in the Y-direction is 3 %. The cells in X- and Z-direction are uniform and the wall distance in the Y-direction is $\triangle y^+_w \approx 0.4$.

3.2. Results and discussion

To quantify the effect of a surface roughness on the flow-wall-interaction, the resulting friction and thus the dissipation of flow energy, the wall shear stress of every surface cell in the computational domain was determined. Higher wall shear stress in turn causes higher dissipation of flow energy. The wall shear stress is the product of the wall-normal gradient of the wall-parallel velocity u_w and the total viscosity μ

$$\tau_W = \mu \frac{\partial u}{\partial n} . \tag{5}$$

To estimate and compare the effect of different surface roughness, the relative change of the wall shear stress (ζ_τ) is determined. For this, the mean values of the local wall shear stresses of the smooth and of the rough surfaces are used

$$\zeta_\tau = \frac{\tau_{w,rough} - \tau_{w,smooth}}{\tau_{w,smooth}} . \tag{6}$$

The results of the two investigations show that the effect of a simulated regenerated surface on the relative change of the wall shear stress is significant, although it appears small. The relative wall shear stress increases to $\zeta_{\tau,kin}= 0.421$ % due to the kinematic simulated surface. The increase of wall shear stress due to the combined kinematic and stochastic surface is $\zeta_{\tau,comb}=1.131$ %, which is significantly higher than for the kinematic surface. Because of the correlation between the wall shear stress, the friction, and the dissipation of flow energy, the combined surface generates higher losses when it is applied to airfoils. This increase results from the distribution of the local wall shear stresses. On the kinematic surface the wall shear stress is homogeneously distributed and only at the peaks of the milling paths the wall shear stress does increase. The wall shear stress on the combined surface is irregularly distributed and is dependent on the local surface shape. Due to the superposition of the stochastic and kinematic surfaces, stronger local maxima and peaks are observed in the combined surface. The interactions of these maxima with the flow yield local maxima in the shear stress, thus raising the overall level of friction.
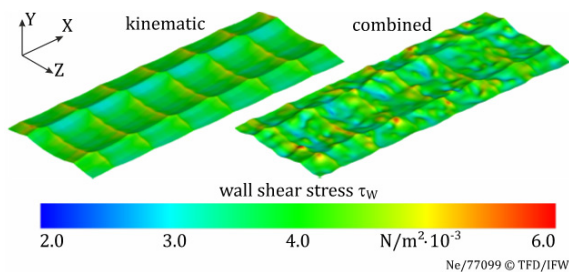

Fig. 8. Results of the numerical studies showing the local wall shear stress distribution on the two different surface topographies on the bottom of the simulated channel

The results show, that in aerodynamic investigations it is important to consider the presented combined approach, including the stochastic topology contribution. This is especially relevant to improve the estimation of the aerodynamic effects, such as the wall shear stress, of regenerated surfaces in simulations.

4. Conclusions

This paper presents a combined simulation for surface topography prediction after milling. It uses a material removal simulation (MRS) to consider all kinematic characteristics of the process as well as an empirical model to predict stochastic influences. The combined simulation shows better prediction capability than the kinematic simulation. A direct numerical simulation of both the kinematic and combined simulated surfaces reveals the importance of the stochastic influence on the flow-wall-interactions. For more general usage in the future the described stochastic method will be adopted to include the microgeometry of the cutting tool, based on the findings of Lavernhe et al. [23].

References

[1] A. Eberlein, Phases of high-tech repair implementation, in: 18th International Symp. on Airbreathing Engines, Beijing; 2007.

[2] M. Bußmann, J. Kraus, E. Bayer, An integrated cost-effective approach to blisk manufacturing, in: 17th Symp. on Airbreathing Engines; 2005.

[3] O. Yilmaz, N. Gindy, J. Gao, A repair and overhaul methodology for aeroengine components, Robotics and Computer-Integrated Manufacturing 2010; 26: 190–201.

[4] L. Markworth, Fünfachsige Schlichtfräsbearbeitung von Strömungsflächen aus Ni-basislegierungen (five-axis finishing of nickelbase airfoils), Ph.D. Thesis, Rheinisch-Westfälische Technische Hochschule Aachen; 2005.

[5] P. P. Knobel, Fräsen von Freiformflächen mit Schleifqualität (milling of free form surfaces with grinding quality), Ph.D. Thesis, Eidgenössische Technische Hochschule Zürich; 2000.

[6] K. Bammert, G. U. Woelk, The influence of the blading surface roughness on the aerodynamic behavior and characteristic of an axial compressor, J. Eng. Power 1980; 102(2): 283–287

[7] M. Arizmendi, et al., Model development for the prediction of surface topography generated by ball-end mills taking into account the tool parallel axis offset. experimental validation, CIRP Annals - Manufacturing Technology 2008; 57(1): 101–104.

[8] N. Liu, M. Loftus, A. Whitten, Surface finish visualisation in high speed, ball nose milling applications, International Journal of Machine Tools and Manufacture 2005; 45(10): 1152–1161.

[9] K.-D. Bouzakis, P. Aichouh, K. Efstathiou, Determination of the chip geometry, cutting force and roughness in free form surfaces finishing milling, with ball end tools, International Journal of Machine Tools & Manufacture 2003; 43: 499–514.

[10] J. Chen, Y. Huang, M. Chen, Study of the surface scallop generating mechanism in the ball-end milling process, International Journal of Machine Tools and Manufacture 2005; 45(9): 1077–1084.

[11] J. P. Bons, A Review of Surface Roughness Effects in Gas Turbines, ASME Journal of Turbomachinery 2010; 132(2)

[12] N. Abuaf, R. S. Bunker, C. P. Lee, Effects of Surface Roughness on Heat Transfer and Aerodynamic Performance of Turbine Airfoils, ASME Journal of Turbomachinery 1998; 120: 522–529

[13] F. Hummel, M. Lötzerich, P. Cardamone, L. Fottner, Surface Roughness Effects in Turbine Blade Aerodynamics, ASME Journal of Turbomachinery 2005; 127: 453–461

[14] Q. Zhang, M. Goodro, P. M. Ligrani, R. Trindale, S. Sreekanth, Influence of Surface Roughness on the Aerodynamic Losses of a Turbine Vane, ASME Journal of Fluids Engineering 2006; 128: 568–578

[15] M. P. Schultz, K. A. Flack, Turbulent boundary layers on a systematically varied rough wall, Physics of Fluids 2009; 21(1)

[16] S. Hohenstein, J. Seume, Numerical Investigation on the Influence of Anisotropic Surface Roughness on the Skin Friction, Proceedings of the European Turbomachinery Conference; 2013

[17] M. Boese, Effects of Riblets on the Loss Behaviour of a Highly Loaded Compressor Cascade, Proceedings of ASME Turbo Expo; 2002

[18] B. Denkena, V. Böß, D. Nespor, A. Samp, Kinematic and stochastic surface topography of machined TiAl6V4-parts by means of ball nose end milling, Procedia Engineering 2011; 19(0): 81–87.

[19] B. Denkena, V. Böß, Technological NC simulation for grinding & cutting processes using cuts, in: 12th CIRP Conference on Modelling of Machining Operations, Donostia-San Sebastián; 2009, p. 563–566.

[20] S. Goeke, S. Rausch, S. Schumann, D. Biermann, Charakterisierung funktionaler Oberflächen durch die konfokale Weißlichtmikroskopie (characterization of functional surfaces using white light confocal microscopy), Forum Schneidwerkzeug- und Schleiftechnik 2013; 88–95.

[21] S. Rusinkiewicz, M. Levoy, Efficient variants of the ICP algorithm, in: Proceedings of the Third Intl. Conf. on 3D Digital Imaging and Modeling; 2001, p. 145–152.

[22] E. Ozturk, L. Tunc, B. E., Investigation of lead and tilt angle effects in 5-axis ball-end milling processes, International Journal of Machine Tools & Manufacture 2009; 49: 1053–1062.

[23] S. Lavernhe, Y. Quinsat, C. Lartique, C. Bown, Realistic simulation of surface defects in five-axis milling using the measured geometry of the tool, Int. Journal of Manufacturing Technology 2014; 74: 393-401

[24] G. J. Hahn, S. S. Shapiro, Statistical Models in Engineering, Wiley Classics Library; 1967.

[25] K. Pearson, Mathematical contributions to the theory of evolution: Supplement to a memoir on skew variation, Philosophical Transactions of the Royal Society A 1901; 197: 443–459.

[26] N. L. Johnson, S. Kotz, N. Balakrishnan, Continuous Univariate Distribution, Volume 1, 2nd Edition, Wiley-Interscience; Volume 1 edition; 1994.

[27] OpenFOAM Foundation, OpenFOAM The Open Source CFD Toolbox, Programmer's Guide (2013)